Quantifying daily versus annual contributions of snowmelt water to streamflow using graphical and geochemical hydrograph separation

Samuel Miller<sup>1</sup>, Steve Lyon<sup>2</sup>, and Scott Miller<sup>3</sup>

July 13, 2020

#### Abstract

In this study, we characterize the snowmelt hydrological response of nine nested headwater watersheds in southeast Wyoming by separating streamflow into three components using a combination of tracer and graphical approaches. First, continuous records of specific conductance (SC) from 2016 to 2018 were used to separate streamflow into direct runoff and baseflow components. Then, diurnal streamflow cycles occurring during the snowmelt season were used to graphically separate direct runoff into quickflow, representing water with the shortest residence time, and throughflow, representing water with longer residence time in the soil column and/or regolith layers before becoming streamflow. On average, annual streamflow was comprised of between 22% to 46% baseflow, 7% to 14% quickflow, and 46% to 55% throughflow across the watersheds. We then quantified hysteresis at both annual and daily timescales by plotting SC versus discharge. Annually, most watersheds showed negative, concave, anticlockwise hysteretic direction suggesting faster flow pathways dominate streamflow on the rising limb of the annual hydrograph relative to the falling limb. At the daily timescale during snowmelt-induced diurnal streamflow cycles, hysteresis was negative, but with a clockwise direction implying that quickflow peaks generated from the concurrent daily snowmelt, with shorter residence times and lower specific conductance, arrive after throughflow peaks and preferentially contribute on the falling limb of diurnal cycles. Slope aspect and surficial geology were highly correlated with the partitioning of streamflow components. South-facing watersheds were more susceptible to early season snowmelt at slower rates, resulting in less direct runoff and more baseflow contribution. Conversely, north-facing watersheds had longer snow persistence and larger proportions of direct runoff and quickflow. Watersheds with surficial and bedrock geologies dominated by glacial deposits had a lower proportion of quickflow compared to watersheds with large percentages of metasedimentary rocks and glaciated bedrock.

## Title Page

- 1. Quantifying daily versus annual contributions of snowmelt water to streamflow using graphical and geochemical hydrograph separation
- 2. Snowmelt contribution to streamflow
- 3. Samuel A ${\rm Miller^{1,2,3}},$ Steven W. Lyon², Scott N.  ${\rm Miller^1}$
- 4. University of Wyoming, Department of Ecosystem Science and Management<sup>1</sup>

Ohio State University, School of Environment and Natural Resources  $^2\mathrm{Corresponding}$  author  $^3$  : miller.10513@osu.edu

Acknowledgements: Funding was provided by NSF-EPSCOR-1208909 and University of Wyoming.

## Main Text File

Quantifying daily versus annual contributions of snowmelt water to streamflow using graphical and geochemical hydrograph separation

<sup>&</sup>lt;sup>1</sup>The Ohio State University

<sup>&</sup>lt;sup>2</sup>Ohio State University

<sup>&</sup>lt;sup>3</sup>University of Wyoming

# Abstract

In this study, we characterize the snowmelt hydrological response of nine nested headwater watersheds in southeast Wyoming by separating streamflow into three components using a combination of tracer and graphical approaches. First, continuous records of specific conductance (SC) from 2016 to 2018 were used to separate streamflow into direct runoff and baseflow components. Then, diurnal streamflow cycles occurring during the snowmelt season were used to graphically separate direct runoff into quickflow, representing water with the shortest residence time, and throughflow, representing water with longer residence time in the soil column and/or regolith layers before becoming streamflow. On average, annual streamflow was comprised of between 22% to 46% baseflow, 7% to 14% quickflow, and 46% to 55% throughflow across the watersheds. We then quantified hysteresis at both annual and daily timescales by plotting SC versus discharge. Annually, most watersheds showed negative, concave, anti-clockwise hysteretic direction suggesting faster flow pathways dominate streamflow on the rising limb of the annual hydrograph relative to the falling limb. At the daily timescale during snowmelt-induced diurnal streamflow cycles, hysteresis was negative, but with a clockwise direction implying that quickflow peaks generated from the concurrent daily snowmelt, with shorter residence times and lower specific conductance, arrive after throughflow peaks and preferentially contribute on the falling limb of diurnal cycles. Slope aspect and surficial geology were highly correlated with the partitioning of streamflow components. South-facing watersheds were more susceptible to early season snowmelt at slower rates, resulting in less direct runoff and more baseflow contribution. Conversely, north-facing watersheds had longer snow persistence and larger proportions of direct runoff and quickflow. Watersheds with surficial and bedrock geologies dominated by glacial deposits had a lower proportion of quickflow compared to watersheds with large percentages of metasedimentary rocks and glaciated bedrock.

Keywords: snowmelt, hydrology, streamflow, watershed, tracer, specific conductance, hydrograph separation, hysteresis

## INTRODUCTION

Rivers draining mountainous regions around the world are vital for supplying water for both consumptive uses and ecosystem services. This is especially true in regions like the Southern Rocky Mountains where the surrounding basins are classified as semi-arid to arid and rely predominantly on mountain runoff to meet water demands. Agriculture in this area, for example, is considered at risk from changing snowmelt patterns associated with global climate change (Qin et al., 2020). In such systems, snow is the dominant form of precipitation, but warming temperatures threaten to decrease annual snowpacks and shift seasonality (IPCC, 2013). Since snowmelt is more efficient than rain at generating streamflow (Li, Wrzesien, Durand, Adam, & Lettenmaier, 2017) and recharging aquifers in many mountainous regions (Earman, Campbell, Phillips, & Newman, 2006; Jasechko et al., 2014), reductions in snowpack pose a potential disruption to the delivery of water to streams and aquifers. Increases in temperature can reduce snowmelt rates (Musselman, Clark, Liu, Ikeda, & Rasmussen, 2017) and snow water equivalent (SWE) (Hamlet, Mote, Clark, & Lettenmaier, 2005), resulting in earlier timing in the onset of streamflow in western North America (Stewart, Cayan, & Dettinger, 2005) and subsequent decreases in summer streamflow (Rood et al., 2008) – potentially leading to habitat loss for endemic species (Lytle & Poff, 2004).

Changes in snowmelt are of course only part of the story for how mountain rivers and streams respond hydrologically under climatic shifts. The time it takes for water to move through a watershed and arrive in streams, thus controlling the shape of the hydrograph, is the result of interactions between precipitation inputs and the eco-physical characteristics of the watershed (Singh, 1997). Variations in vegetation composition (Molotch et al., 2009; Vivoni et al., 2008), topography (Broxton, Troch, & Lyon, 2009; Webb, Fassnacht, & Gooseff, 2018), and the lithology and structure of underlying soil and geologic formations (Mueller, Weingartner, & Alewell, 2013; Nippgen, McGlynn, Marshall, & Emanuel, 2011) can influence the residence time and flow pathways of water in concert thereby impacting both the quality and quantity of water arriving in streams.

Detangling such interactions is particularly challenging in mountainous regions given the complexity and remoteness of the landscapes (e.g. Jantze, Laudon, Dahlke, & Lyon, 2015). Still, efforts to characterize older groundwater contributions to streamflow (i.e. baseflow) in snowmelt-dominated headwater mountains regions serve to increase our understanding on how groundwater interacts with the environment and has important implications for the vulnerability of water resources and ecosystems under warming conditions (Miller, Buto, Susong, & Rumsey, 2016). The effect of the underlying geologic formations becomes most apparent during dry weather and baseflow conditions, when direct runoff has drained and streamflow comes from older groundwater sources (Cross, 1949). Understanding how groundwater contributions to streamflow are affected by different geologies is needed given that increasing temperatures have shown to reduce runoff efficiency (the ratio of runoff to precipitation) in watersheds near our study area (McCabe, Wolock, Pederson, Woodhouse, & McAfee, 2017).

Hydrologists have established numerous methods for separating hydrographs for well over 150 years. For example, Hall (1968) provides a thorough review on early attempts to model baseflow using graphical or mathematical approaches. Graphical approaches continue to be popular choices in data-limited regions as they only require observation of streamflow (Mugo & Sharma, 1999; Reitz, Sanford, Senay, & Cazenas, 2017). Collection of specific source-water chemical and / or isotopic composition allows for mass-balance (tracer-based) approaches for separating hydrographs into various flow components (Pinder & Jones, 1969). Mass-balance approaches are considered more reliable, particularly in mountainous regions, compared to graphical or mathematical interpretations because they integrate watershed-specific geochemical information (Miller, Susong, Shope, Heilweil, & Stolp, 2014). However, success using mass-balance methods to separate hydrograph components hinges on the ability to accurately assign concentrations to end-members. Combining graphical and tracer techniques offers a potentially cost-effective approach that has proven beneficial in identifying dominant underlying processes that would not have been possible with one method alone (Kronholm & Capel, 2015; McNamara, Kane, & Hinzman, 1997).

One example of where both tracer and graphical hydrograph separations might be complimentary is in the snowmelt-dominated and seasonally arid Snowy Range of southeast Wyoming, USA. In such systems, specific conductance (SC), a measurement of the ionic content in water, provides a strong natural tracer due to the large differences in concentration observed between peak flow and low flow conditions (Miller et al. , 2014). Further, SC can be measured continuously at relatively low costs using automated loggers, provides the best hydrograph separation results compared to individual chemical constituents (Caissie, Pollock, & Cunjak, 1996), and has been used successfully to separate baseflow in similar watersheds in the Southern Rocky Mountains (Caine, 1989; Liu, Williams, & Caine 2004; Miller et al., 2014; Rumsey, Miller, Susong, Tillman, & Anning, 2015). In addition, given the strong diurnal responses of Rocky Mountain systems to snowmelt "pulses", graphical techniques might have utility to isolate changes in the fast flow pathways as the snowmelt season progresses and snowpack depletes (Buttle, Webster, Hazlett, & Jefferies, 2019). Diurnal streamflow cycles have been previously analyzed to gain process understanding on the hydrologic response to snowmelt (Caine, 1992; Kobayashi, 1986; Kurylyk & Hayashi, 2017; Loheide & Lundquist, 2009; Lundquist & Cayan, 2002; Lundquist & Dettinger, 2005; Mutzner et al. , 2015; Pellerin et al. , 2012; Woelber et al. , 2018).

The goal of this study is to assess the storage and release of snowmelt by quantifying the relative proportions of quickflow, throughflow, and baseflow contributions to streamflow. We do this for nine nested watersheds of the Snowy Range in southeastern Wyoming, USA by estimating how various sources contributed to discharge under different streamflow conditions throughout the year (i.e. rising limb, peak flow, falling limb, low flow). We used a common chemical mass-balance method to separate baseflow from direct runoff (Pinder & Jones, 1969). Direct runoff was further separated into throughflow and quickflow graphically based on naturally occurring diurnal cycles in streamflow that reflect rapid additions of direct runoff to streamflow induced by daily fluctuations in temperature. Further, we compared SC-Q hysteresis at both annual and daily timescales with watershed characteristics to better elucidate runoff processes driving the streamflow partitioning. Specifically, we address the following research questions for our seasonally-arid, snow-dominated systems:

- 1. How do the sources of streamflow differ between seasonal and annual timescales?
- 2. How do SC-Q relationships reflect the storage and release of snowmelt water at daily and annual scales?
- 3. What are the dominant watershed properties governing streamflow partitioning and SC-Q relationships?

# SITE DESCRIPTION AND DATA COLLECTION

## 2.1 Site description

The Snowy Range is the northernmost extent of the Medicine Bow Mountain Range within the Southern Rocky Mountains. We installed stream monitoring sites at nine nested locations along Libby Creek and the North Fork of the Little Laramie and their tributaries (Figure 1; Table 1). Data considered in this study were collected during three consecutive water years (October to September) covering 2016 through 2018. Our study watersheds range in elevation from 2570 – 3619 m (8431 – 11874 ft) and areal extent from 0.53 to 63.0 km<sup>2</sup>. The watersheds drain predominantly south and east towards Centennial, WY about 50 km east of Laramie, WY.

Bedrock geology underlying the watersheds is primarily a mix of metasedimentary and metavolcanic from the Early Proterozoic and glacial deposits from the Pleistocene-Holocene (Figure S1; Table S1; Wyoming State Geological Survey, 2014). Metasedimentary rocks from the Libby Creek Group are most prevalent at higher elevations consisting of metaclastic quartzite, politic and amphibole-schist, with minor traces of marble and conglomerate. Metasedimentary and metavolcanic rocks are common in GOLD100. Lower elevations of LIBB100 contain politic-schist, gneiss, and amphibolite with minor amounts of marble and granite. Glacial deposits consisting of unconsolidated, coarse-detrital gravel, boulders, and sand are common in the region. Landslide deposits occur in portions of NFLL100 containing intermixed glacial deposits, talus, and rock-glacier deposits. The surficial geology is dominated by glacial deposits lower elevations (Figure S2; Table 2; Case, Arneson, & Hallberg, 1998). Glacial deposits consist of scattered slope wash, residuum, grus, alluvium, colluvium, and landslide deposits. Glaciated bedrock is more common at higher elevations mixed with scattered shallow eolian, grus, colluvium, and alluvium deposits. Grus and residuum mixed with alluvium dominate the surficial geology of GOLD100, an outlier compared to the other study watersheds.

No detailed soil map has been constructed for our study watersheds. Munn and Arneson (1998) performed a low-order assessment and found soils to be highly variable, both regionally and locally with changes in slope aspect, slope position, climate, and geology. Haplocryalfs and Dystrocryepts occupy most of the area. Haplocryalfs tend to occur on low-relief areas while Dystrocryepts occupy forests on glacial deposits and on steep slopes. Cryaquepts and minor histisols are present in riparian areas (Munn & Arneson, 1998). Seismic refraction surveys performed in NONM100 indicate thin regolith at the top of hillslopes (1 m) thickening toward the bottom of the slope (3-4 m; Thayer et al., 2018). A porosity transition within the regolith indicated by seismic refraction surveys suggests the top layer of upper regolith has relatively high hydraulic conductivity capable of draining quickly. A novel bulk density optimization method performed in NONM100 supports the decline in porosity with depth, which creates conditions that favor shallow lateral flow through the upper regolith as a dominant streamflow generation mechanism (Fullhart, Kelleners, Chandler, McNamara, & Seyfried, 2019).

Evergreen forest is the main land cover classification in eight of our nine study watersheds ranging from 30 % (LIBB100) to 99 % (NONM100) coverage and is more common at lower elevations (Figure S3; Table S2; Homer & Fry, 2016). Shrub/scrub and grassland/herbaceous coverages with intermittent lakes and wetlands tend to dominate at higher elevations.

#### 2.2 Data collection

# 2.2.1 Snow and climatological monitoring

The study watersheds receive most of their annual precipitation in the form of snow. Spring snowmelt, typically occurring in a relatively short period of time after the snowpack has become 'ripe', is a main driver of streams. Snow water equivalent (SWE) was recorded at six stations in our study watersheds (Figure 1). The Brooklyn Lake SNOTEL (sitenumber = 367) site is located within the boundaries of NASH200. According to 30-year daily median records (1981-2010), maximum SWE occurs on April 30 with a value of 59.2 cm. Mean water year total precipitation for Brooklyn Lake is 89.7 cm, which results in a mean water-year snow fraction (maximum SWE / total precipitation) of 66%. During the three-year period presented in this study, maximum SWE was remarkably consistent from 2016 to 2018 at the six measurement sites (Table S3). On average, maximum SWE ranged from about 32 cm at the lowest site (2684 m) to 72 cm at the highest site (3244 m) (Table S3).

Snow depth in 2016 was calculated at 0.5-m resolution in our study watersheds using LIDAR data based on two flights: snow-free in October 2014 and peak snow depth in April 2016 (Table S4). Monthly precipitation and temperature data from PRISM were aggregated to watershed boundaries to provide water-year (Oct. 1 – Sept. 30) mean watershed precipitation and temperature estimates (Table S4) (PRISM Climate Group, 2019). Water-year precipitation from PRISM (2016) was highly correlated to LIDAR-derived snow depth and elevation (Pearson's r = 0.98, 0.99, respectively).

### 2.2.2 Stream monitoring

Stream stage (Level TROLL 500 Data Logger, In-Situ, Fort Collins, CO, USA; accuracy =  $\pm$  0.05%, resolution =  $\pm$  0.005%), electrical conductivity (ONSET HOBO U24, Onset Computer Corporation, Bourne, MA, USA; accuracy = 5 µS/cm, resolution = 1 µS/cm), and temperature (ONSET HOBO U24, Onset Computer Corporation, Bourne, MA, USA; accuracy = 0.1 °C, resolution = 0.01 °C) were measured instantaneously at 15 min intervals at nine gaging locations in the Snowy Range from 2016 to 2018 (Figure 1). Streamflow was estimated by creating rating curves at each gaging location that relate measured stream stage to repeated field measurements of discharge using a handheld electromagnetic water flow meter (OTT MF pro, OTT HydroMet, Loveland, CO, USA; accuracy =  $\pm$  2%). Electrical conductivity was measured by automated loggers and converted to specific conductance (SC) to account for differences in stream temperature following methodology from the manufacturer.

Stream stage and electrical conductivity loggers were installed each year prior to the main snowmelt period, but at slightly different dates for each gaging site. To account for variability in record length we calculated cumulative streamflow for each water year at each site and only analyzed the records after 3% of annual streamflow had occurred. This approximation allowed for consistent inter-site and inter-annual comparisons. Each year of analysis concluded at the end of the water year (September 30). Four periods were selected from the total hydrograph to assess dominant controls of runoff generation at different hydrologic conditions: the rising limb, peak flow, falling limb, and low flow conditions. The rising limb encompasses the time between the beginning of the snowmelt period of the hydrograph (defined in below in 'Graphical quickflow separation') and the date of maximum discharge. The peak flow time period was selected based on the highest 10% of streamflow values. The falling limb occurs between the date of maximum stream discharge and the last day of the snowmelt period of the hydrograph. It should be noted that based on these definitions peak flow partially overlaps with the rising and falling limbs. The low flow time period refers to the lowest 30% of streamflow recorded after the snowmelt portion of the hydrograph.

# **METHODS**

# 3.1 Hydrograph separation

# 3.1.1 Tracer-based separation

We followed a chemical mass-balance methodology from Pinder & Jones (1969) for a tracer-based approach to separate baseflow and direct runoff from the total hydrograph:

$$C_T Q_T = C_{BF} Q_{BF} + C_{DR} Q_{DR}(1)$$

Where C and Q represent concentration and discharge, respectively, and subscripts T, BF, and DR refer to total, baseflow, and direct runoff, respectively. For this study, we use SC as the "concentration" of interest in Eq. (1) (e.g. Caine, 1989; Kobayashi, 1986; Miller et al., 2014; Pilgrim, Huff, & Steele, 1979). The quantity of baseflow can be solved by rearranging Eq. (1):

$$Q_{\rm BF} = Q_T \left[ \frac{C_T - C_{\rm DR}}{C_{\rm BF} - C_{\rm DR}} \right] (2)$$

Accurate interpretation of Eq. (2) requires that the following assumptions are made (Sklash & Farvolden, 1979; Buttle, 1994): (1) direct runoff and baseflow have different chemical composition, (2) direct runoff and baseflow chemical compositions are constant in time and space or the variability can be accounted for, (3) soil water contribution to streamflow is small or has similar composition of direct runoff, and (4) surface storage has a minor contribution to streamflow. Total stream concentration ( $C_T$ ) and discharge ( $Q_T$ ) are obtained using in-situ measurements. The baseflow concentration ( $C_{BF}$ ) is typically estimated from low flow stream conditions when total streamflow is assumed to be entirely derived from groundwater. We followed suggestions from Miller et al. (2014) and calculated  $C_{BF}$  at each watershed by selecting the 99<sup>th</sup> percentile of the SC data to account for potential outliers. We assigned  $C_{DR}$  a value of 21.6 μS/cm based on the mean value measured from 13 snow and 10 snowmelt samples. The SC of these samples ranged from 9.8 μS/cm to 42.1 μS/cm and the standard deviation across all 23 samples was 10.5 μS/cm.

Uncertainty was quantified following methods presented by Genereux (1998):

$$W_{\rm BF} = \sqrt{\left(\frac{f_{\rm BF}}{C_{\rm DR} - C_{\rm BF}} W_{C_{\rm BF}}\right)^2 + \left(\frac{f_{\rm DR}}{C_{\rm DR} - C_{\rm BF}} W_{C_{\rm DR}}\right)^2 + \left(\frac{-1}{C_{\rm DR} - C_{\rm BF}} W_{C_T}\right)^2} (3)$$

where  $W_{BF}$  represents the uncertainty in baseflow discharge to streamflow at the 95% confidence interval,  $f_{BF}$  and  $f_{DR}$  are the fractions of total streamflow from baseflow and direct runoff, respectively,  $W_{C_{BF}}$  is the standard deviation of the highest 1% of measured SC concentrations multiplied by the t-value from the Student's t distribution,  $W_{C_{DR}}$  is the standard deviation associated with observations of  $C_{DR}$  (21.8  $\mu$ S/cm) multiplied by the t-value, and  $W_{C_T}$  is the analytical error in the SC measurement multiplied by the t-value.

#### 3.1.2 Graphical separation

After separating total streamflow into baseflow and direct runoff using the tracer-based approach, we applied a graphical hydrograph separation technique based on the presence of natural snowmelt-induced diurnal cycles to differentiate direct runoff into two components: throughflow and quickflow. Quickflow runoff represents water that moves most rapidly to the stream channel resulting in sharp rises of the daily hydrograph (Hewlett & Hibbert, 1967; Buttle et al., 2019). Quickflow is generated during the snowmelt period as the result of daily fluctuation in temperature creating diurnal snowmelt pulses (Caine, 1992). For this reason, we constricted quickflow to only occur at times of peak snowmelt based on when the moving-average seven-day runoff was greater than 0.5 times mean water year daily runoff (i.e. the snowmelt period). This procedure approximated the time when snowmelt-induced diurnal cycles were present. The residual of the direct runoff water not contributing to quickflow was assumed to be throughflow, which represents delayed flow interacting more with the subsurface, resulting in a longer travel time.

A computer code was written to identify diurnal cycles by selecting times when instantaneous streamflow curvature was at a daily maximum. Quickflow volumes were calculated by subtracting the area created above the diurnal snowmelt cycles from the total hydrograph. The diurnal cycle (%) was then calculated by dividing the difference between daily maximum and minimum streamflow by the daily maximum streamflow for each day in the snowmelt period. Visual inspection of each hydrograph was performed to ensure accurate snowmelt period selection and quickflow volume calculation.

#### 3.2 Hysteresis index

An index was calculated to quantify specific conductance-discharge (SC-Q) hysteresis at annual and daily scales during snowmelt-induced diurnal cycles. We adopted methodology from Lloyd, Freer, Johnes, and Collins (2016) who suggest rescaling the SC and Q data through minimum-maximum normalization to allow for an index that represents changing dynamics of an event and permits comparison between events:

Normalized 
$$Q_i = \frac{Q_i - Q_{\min}}{Q_{\max} - Q_{\min}}$$
 (4) Normalized  $SC_i = \frac{SC_i - SC_{\min}}{SC_{\max} - SC_{\min}}$  (5)

Normalized  $Q_i = \frac{Q_i - Q_{\min}}{Q_{\max} - Q_{\min}}(4)$ Normalized  $SC_i = \frac{SC_i - SC_{\min}}{SC_{\max} - SC_{\min}}(5)$ where  $Q_i$  and  $SC_i$  represent discharge and specific conductance at time i,  $Q_{\min}$  and  $SC_{\min}$  are the minimum discharge and specific conductance, and  $Q_{max}$  and  $SC_{max}$  are the maximum discharge and specific conductance. The hysteresis index (HI) is calculated by subtracting the normalized SC on the falling limb from the normalized SC on the rising limb for a particular flow percentile:

$$\mathrm{HI}_{Q_i} = \mathrm{Normalized} \ \mathrm{SC_i}_{\mathrm{Rising\ limb}} - \mathrm{Normalized} \ \mathrm{SC_i}_{\mathrm{Falling\ limb}}(6)$$

At the annual scale, we calculated a hysteresis index for the 10<sup>th</sup>, 25<sup>th</sup>, and 50<sup>th</sup> percentile of discharge values. For example, HI10 was calculated by subtracting the tenth percentile of discharge occurring during the falling limb from the tenth percentile of discharge occurring during the rising limb.

The HI varies between -1 and 1, where the larger the absolute value indicates a more circular hysteresis and the sign represents the direction of the loop (positive for clockwise, negative for counter-clockwise) (Lloyd et al., 2016). To avoid spikes in the data affecting the hysteresis index, we averaged the normalized SC for values within 1% of each annual hysteresis index percentile (i.e. the 10<sup>th</sup> percentile of normalized discharge was expanded to include the 9<sup>th</sup> through 11<sup>th</sup> percentile values).

Similar methodology was applied to create a hysteresis index at the daily scale. For this analysis, each date was rescaled from noon on the particular date to noon on the subsequent date because snowmeltinduced diurnal cycles begin rising in the late afternoon following a delay from the time of peak daily solar maximum. The daily hysteresis index was calculated for the 25<sup>th</sup>, 50<sup>th</sup>, and 75<sup>th</sup> percentile of normalized discharge values. Due to many fewer data points compared to the annual datasets, we expanded the buffer by averaging the normalized SC for values within 10% of each daily hysteresis index percentile (i.e. the 25<sup>th</sup> percentile of normalized discharge was expanded to include the 15<sup>th</sup> through 35<sup>th</sup> percentiles).

# 4. RESULTS

# 4.1 Tracer-based hydrograph separation

Baseflow contributions to streamflow varied spatially and temporally but were greatest at low flow conditions for all watersheds (Figure 2; Table 3). On average, total baseflow contributions to streamflow in the study watersheds ranged from 22.1% (GOLD100) to 45.5% (NONM100). This range of baseflow contribution is similar to other studies in the Upper Colorado River Basin (Miller et al., 2014; Rumsey et al., 2015). During the rising limb portion of the annual hydrograph, baseflow contributions ranged from 14.2% (GOLD100) to 33.9% (NFLL200). Baseflow contributions were lowest during peak flow conditions, ranging from 10.8% (GOLD100) to 29.0% (NASH100). During the falling limb, proportions of baseflow increased slightly and ranged from 13.0% (GOLD100) to 32.8% (NASH100). Baseflow contributions to streamflow were greatest at low flow conditions and ranged from 65.6% (NASH100) to 93.4% (GOLD100) (Table 3). The close proximity of NASH100 to Brooklyn Lake, which is one of the largest lakes in the region and is located upstream of NASH100, likely explains the smaller contribution of baseflow to total streamflow at low flow conditions.

Uncertainty was greater when proportions of direct runoff were greater due to a smaller, and more variable, number of snowmelt/snowpack samples used to define  $C_{DR}$  in Eq. 3 (Table 3).

It is important to emphasize that most of the total streamflow in our study watersheds was generated during a relatively brief period associated with peak snowmelt. The highest 10% of recorded streamflow values (i.e. peak flow conditions) were responsible for 37% (NASH200) to 47% (GOLD100, LIBB200, LIBB400) of total streamflow in our study watersheds (Table 4). During this time, streamflow was overwhelmingly derived from direct runoff (Table 3). In contrast, the lowest 30% of streamflow values recorded after peak flow (i.e. low flow conditions) accounted for only 1.4% (LIBB100, LIBB200) to 3.0% (NFLL100) of total streamflow (Table 4) and were primarily sourced from baseflow (Table 3). However, baseflow contributions were responsible for a majority of total streamflow generation on any particular day outside of the relatively short snowmelt period.

# 4.2 Graphical hydrograph separation

Direct runoff produced during diurnal snowmelt cycles (Figure 3) resulted in quickflow contributions to total streamflow that ranged from 7% (NASH100) to 14% (LIBB100, LIBB200) annually (Table 4). Quickflow was responsible for 15.4% (NASH100) to 27.7% (LIBB100) of direct runoff during the snowmelt period and 11.4% (NASH100) to 22.1% (LIBB200) of direct runoff annually for our study watersheds (Table 5). When present, the mean snowmelt-induced diurnal streamflow cycle ranged from 19.7% (NASH100) to 33.5% (LIBB100) of total streamflow during the snowmelt period (Table 5). The mean magnitude of the diurnal cycle was significantly (p < 0.05) greater for Libby Creek (LIBB100, LIBB200, LIBB400) compared to Nash Fork and the North Fork of the Little Laramie (NASH100, NASH200, NFLL100, NFLL200). Throughflow was the main contributor to streamflow at all times except during low flow conditions (Figure 4; Tables 4 & 5) when baseflow was dominant. The close proximity of NASH100 to Brooklyn Lake, which drains directly to the Nash Fork main channel, likely dampened the amplitude of the diurnal fluctuations measured in the stream and resulted in the lowest proportion of quickflow of all the watersheds considered.

#### 4.3 Annual SC-Q hysteresis

Discharge (Q) and SC generally mirror each other in our study watersheds with the highest Q values corresponding with the lowest SC (and vice versa) implying dilution from snowmelt water with low SC at high Q (Figure 5). Time lags between SC and Q at an annual scale result in hysteresis which varies systematically across the different runoff components. In NONM100, LIBB100, LIBB200, and LIBB400, SC-Q relationships have a negative, concave, and anticlockwise hysteretic behavior at annual timescales, resulting in negative annual hysteresis indices (Figure 5d; Table 6), implying that SC concentration is greatest in baseflow, followed by throughflow, and then quickflow (Evans & Davies, 1998). The lack of annual hysteresis observed at GOLD100, NASH100, and NFLL100 implies little to no time lag between annual peak SC and annual peak Q suggesting relatively inert subsurface material properties that result in little chemical evolution as water travels through the soil and /or regolith layers. Thus throughflow and quickflow result in similar geochemical alteration in these watersheds (Figure 5c).

All watersheds had a negative relationship between SC and Q on an annual scale, implying recently melted snow (i.e. from the current snowmelt season) is responsible for the majority of streamflow generation in a given year. Seasonal snowmelt has been shown to be the dominant streamflow generation mechanism in the western United States (e.g. Li et al. , 2017) but differs from what has been shown using isotope tracers in snowmelt-dominated watersheds located in lower-elevation, humid areas (e.g. Buttle, 1994; Laudon, Sjoblom, Buffam, Seibert, & Morth, 2007) where snowmelt mainly recharges groundwater and displaces previously stored older water.

## 4.4 Daily SC-Q hysteresis

When distinct snowmelt-induced diurnal streamflow cycles are present, Q and SC often demonstrated daily hysteresis. The shape of the diurnal streamflow cycle was typically front-loaded, where streamflow rises

rapidly followed by more gradual decline (Figure 6a). The opposite was true for SC in streamflow which exhibited a sharp drop followed by a gradual increase (Figure 6a). This phenomenon was also demonstrated by Kobayashi (1986) during snowmelt in the headwaters of the Uryu River, Japan. In most observed cases for our study watersheds, SC was lower on the falling limb of diurnal cycles than on the rising limb, resulting in clockwise hysteresis and positive daily hysteresis indices (Figure 6b-c; Table 6). The daily hysteresis index was largest on the rising limb of the annual hydrograph for most watersheds (Figure 6b; GOLD100, NASH100, NASH200, NFLL200, NONM100) and became smaller throughout the snowmelt period during the falling limb of the annual hydrograph (Figure 6c). The opposite was true for Libby Creek watersheds (LIBB100, LIBB200, LIBB400), where the hysteresis index became larger as the snowmelt period progresses.

## 4.5 Relating SC-Q hysteresis, streamflow components and watershed properties

On an annual scale, we detected a significant negative correlation between quickflow proportion and the mean annual hysteresis index at the  $50^{\rm th}$  percentile of discharge values (Table 7; Pearson's r = -0.77, p-value < 0.05). Watersheds with higher proportions of quickflow tended to have larger negative hysteresis indices implying these watersheds behaved the flashiest in response to diurnal snowmelt pulses. The other runoff generation mechanisms (baseflow and throughflow) were not correlated to any of the annual hysteresis indices, supporting evidence that the youngest fraction of runoff controls stream water solute concentration dynamics (Benettin et al. , 2017).

We found strong relationships between direct runoff partitioning (i.e. throughflow vs quickflow) and slope aspect of our study watersheds. Watersheds with more land area facing north were associated with greater annual proportions of quickflow (Table 7; Pearson's r=0.72, p-value <0.05). North-facing aspects tend to receive less direct radiation, and snowpacks persist longer compared to south-facing slopes. This allows snowpacks to melt later in the year at higher temperatures and thus faster rates (Musselman et al. , 2017), which brings about conditions favorable for quickflow. Longer persistence of snowpacks on north-facing slopes leads to the development of preferential meltwater flowpaths at the snow-soil interface, resulting in as much as 170% more snow water equivalent accumulating along the length of north-facing hillslopes compared to south-facing hillslopes (Webb et al. , 2018).

The percentage of surficial geology covered with glacial deposits was significantly negatively correlated to the proportion of annual streamflow derived from quickflow (Table 7; Pearson's r = -0.66, p-value < 0.05). Watersheds with low proportions of quickflow (NASH100, NASH200, NFLL100, NFLL200) had a larger percentage of glacial deposits covering their surficial and bedrock geologies (Tables 2, 4 & S1). In contrast, watersheds with larger proportions of quickflow tended to have bedrock geology dominated by metasedimentary and metavolcanic rocks associated with the Libby Creek Formation (Table S1) and surficial geology dominated by glaciated bedrock (Table 2). Glacial deposits were assumed to have higher infiltration capability and thus more drainage capacity thereby reducing the occurrence of quickflow relative to the bedrock associated with the Libby Creek Formation. This bedrock can be considered to have lower infiltration capacity, increasing the occurrence of quickflow.

The percentage of surficial geology covered by glacial deposits was significantly correlated to annual and daily hysteresis indices (Table 7). Watersheds with a higher proportion of glacial deposits tended to produce large, positive hysteresis indices. Waters flowing through glacial deposits, compared to glaciated bedrock, likely have longer residence times and thus more potential geochemical evolution before arriving as streamflow. These factors would lead to more variability in flowpath development and larger hysteresis indices observed at annual and daily scales.

# 5. DISCUSSION

## 5.1 Dominant controls on hydrologic response

Using continuous records of SC and Q we showed that direct runoff (quickflow and throughflow) contributes the majority of the total annual streamflow - especially during the snowmelt period (Table 3). These results

align with other investigations near our study area that used SC (Miller et al., 2014; Rumsey et al., 2015) or stable water isotopes (Huth, Leydecker, Sickman, & Bales, 2004; Liu et al., 2004; Williams, Seibold, & Chowanski, 2009) for hydrograph separation. Hydrograph components were significantly correlated to aspect and surficial geology, while elevation was highly positively correlated to snow depth, mean precipitation, total runoff, and runoff ratio (Table 7). The strong link between elevation and precipitation has been well documented in other mountainous environments that span large elevation ranges (Elder, Dozier, & Michaelsen, 1991). At smaller scales, however, slope aspect impacts the ability of wind to redistribute snow (Dadic, Mott, Lehning, & Burlando, 2010) and vegetation structure significantly alters snow accumulation and ablation patterns (Varhola, Coops, Weiler, & Moore, 2010).

Streamflow and SC data from our watersheds indicated a combination of geology, topography, and precipitation inputs strongly affect the hydrologic response in snow-dominated, headwater catchments (Segura et al. , 2019). As temperatures warm, snowmelt will initiate earlier in the season at slower rates (Musselman et al. , 2017) which could bring about a slower hydrologic response and less near-surface saturation, favoring groundwater recharge and less direct runoff. We can already see evidence of this in our system where watersheds that have more south-facing area are associated with greater proportions of baseflow. Differences in slope aspect will be amplified in the future when snowmelt occurs at earlier dates and the sun angle is lower (Lundquist & Flint, 2006). In future warming scenarios, shaded hillslopes will provide habitat to native species that developed under cooler, wetter scenarios, whereas sunnier areas will be more susceptible to drought and invasion from non-native species.

For the watersheds studied here, longer snow persistence on north-facing or heavily shaded hillslopes enabled high snowmelt rates which bring soils to field capacity and facilitates rapid shallow subsurface flow and return flow (Dunne & Black, 1971). Water typically exfiltrated near the break in slope where hillslopes are adjacent to riparian areas, supporting the variable source area concept (Hewlett, 1961). Return flow exfiltrating from soil and regolith layers is an important contributor to groundwater recharge and has been shown to be resilient to drought and can buffer recharge under climate change (Carroll et al. , 2018). Conversely, south-facing slopes receive more direct radiation during snowmelt compared to north-facing slopes such that snowmelt is typically initiated earlier in the year. This likely contributes to the low percentages of quickflow produced in the watersheds with the greatest percentage of south-facing area (Table 4). This interpretation is consistent with the results from Thayer et al. (2018). Using time-lapse electrical resistivity tomography, they showed the preference for deep drainage occurring on a south-facing hillslope located within NONM100 and concluded that overland flow and lateral shallow-subsurface interflow (i.e. quickflow) were negligible on south-facing hillslopes.

Interestingly, two of our smaller study watersheds and the two lowest total streamflow producing sites (GOLD100 and NONM100; Table 4) had remarkably different runoff generation mechanisms from one another (Figures 2 & 5; Tables 3 & S5). Baseflow contributions during snowmelt were the smallest for the GOLD100 watershed while baseflow contributions were the largest during low flow conditions. This shift in baseflow dominance, from low proportions during high discharge to high proportions during low discharge, suggests that a smaller groundwater storage capacity exists for this watershed. The surficial geology of GOLD100, which is dominated by grus mixed with alluvium, residuum, slopewash and colluvium, is remarkably different than the other study watersheds and likely helps explain the hydrologic response (Table 2). Unlike the other study watersheds, the Libby Glacier only overlaid a small portion of this watershed (Atwood, 1937), resulting in few glaciated deposits which we expect have greater infiltration capacity and the ability to store more water which leads to more geochemical evolution compared to the surficial geology units present in GOLD100 which resulted in a flashy hydrograph behavior during snowmelt.

In contrast, the surficial geology in NONM100 is almost entirely glaciated deposits. The stream draining this watershed received a more constant source of baseflow throughout the year, implying groundwater is an important and stable source of stream water in this small catchment (Carroll, Deems, Niswonger, Schumer, & Williams, 2019). Reductions in snowpack, the primary water storage component in runoff-dominated watersheds like GOLD100, will be more disruptive to the natural flow regime in these types of catchments,

resulting in a larger contraction of the stream network compared to streams that are more groundwater dominated (Tague, Grant, Farrell, Choate, & Jefferson, 2008). Reductions in late season flow and subsequent contraction of the stream network, for example under climatic shifts in seasonality, could potentially reduce aquatic habitat heterogeneity and stream macroinvertebrate biodiversity (Brown, Hannah, & Milner, 2007).

# 5.2 Specific conductance – discharge relationships reflect the storage and release of snowmelt water

While the SC-Q relationship remained consistently negative at annual and daily scales, the direction of hysteresis during snowmelt-induced diurnal cycles (clockwise) was opposite of the direction observed at the annual scale (anti-clockwise). The clockwise hysteretic behavior observed on a daily scale suggested throughflow, with its greater SC and relatively longer residence time, was first flushed out of hillslopes, followed by freshly melted snow, with lowest SC and shortest residence times, that filled in pore space occupied by the discharged throughflow. This behavior supports threshold behavior for runoff generation, where connectivity must be achieved before daily meltwater with the lowest SC contributes to streamflow (Tromp-Van Meerveld & McDonnell, 2006).

In watersheds with the largest mean daily hysteresis index (NFLL100 and NFLL200) the shape of the daily SC – Q hysteresis during snowmelt-induced diurnal cycles was relatively circular during the rising limb and became flatter during peak flow and falling limb conditions (Figure 7). This behavior was documented by Kobayashi (1986) and was attributed to an increase in the subsurface component of streamflow after a snow-free area emerged adjacent to the stream channel. Our results from this change in hysteretic shape support evidence that greater flow pathway variability was present during early snowmelt where water was moving through both relatively shallow and deep flow pathways. During the falling limb, less snow was present in the watershed and throughflow from relatively deeper flow pathways draining soil and regolith layers combined with baseflow were primarily responsible for streamflow generation. This dominance of deeper flow pathways leads to SC values measured in streamflow that vary more linearly related to discharge over daily timescales.

#### 5.3 Potential limitations and future work

Based on field observations in our study watersheds, it is obvious that the vast majority snowmelt infiltrates the ground surface for a period of time. We make no distinction between surface (i.e. overland flow) and subsurface runoff in the nomenclature of our selected hydrograph components based on extensive field observations. During peak snowmelt conditions, water stored in hillslopes was rapidly transported via lateral flowpaths arising from macropores and / or interfaces between depositional units with large density contrasts (Fullhart et al., 2019; McNamara, Chandler, Seyfried, & Achet, 2005; Roberge & Plamondon, 1987; Uchida, Tromp-Van Meerveld, & McDonnell, 2005; ) indicative of threshold runoff response (Penna, Tromp-Van Meerveld, Gobbi, Borga, & Dalla Fontana, 2011; Spence, 2007; Tromp-Van Meerveld & McDonnell, 2006). This quick moving lateral runoff was observed in NONM100 with low SC, exfiltrating from the base of hillslopes where fully saturated riparian areas could not accommodate additional subsurface flow (Figure S4).

As mentioned before, interpretation of our SC-based baseflow hydrograph separation hinges on the ability to accurately assign concentrations to end-members. Due to the fact that SC concentrations are effectively constant throughout the low flow period, we believe the selection of the baseflow end-member is fairly accurate. However, relatively few snow and snowmelt samples were used to assign the direct runoff component. Extensive field mapping and SC measurements of the stream network expansion and contraction in NONM100 during snowmelt revealed that exfiltrated shallow subsurface flow (i.e. return flow) often had an SC concentration similar to or lower than the value assigned to the direct runoff component (21.6  $\mu$ S/cm; Figure S4). We were surprised by the lack of geochemical evolution of this fast-moving return flow and hypothesize that water flowing along these flowpaths had the shortest residence times. The value we assigned to the direct runoff component is in between two values chosen assigned by Miller et al. (2014) (10 and 33  $\mu$ S/cm). Assigning a lower value to our direct runoff end-member would have had little implications to our results

since the difference between direct runoff and baseflow SC is so large in our study watersheds.

Persistent streamflow occurs in all watersheds throughout the winter, except perhaps GOLD100 and NONM100 (not shown). In most of the watersheds stream stage and SC data are constant, indicating stable sources of baseflow contribution during the winter. Unfortunately, like many other similar studies, we collected data only during the relatively warm period of the year when ice is less likely to affect data quality and freezing is less likely to damage equipment. Our results are, for example, underrepresenting the amounts and proportions of baseflow by only using data from the relatively warm period of the year where data collection is more feasible.

While SC is a robust measurement of concentration and automated loggers can record instantaneous values at relatively low costs, information is lost when solute concentrations are aggregated together. Many studies have shown that concentration-discharge relationships vary for different individual solutes (e.g. Lewis & Grant, 1979; Godsey, Kirchner, & Clow, 2009). Exploring individual solute concentration-discharge relationships may help refine our knowledge on the number of different flow pathways water may take before arriving as streamflow. Further, stable water isotope composition sampled from our study watersheds did not permit the use of hydrograph separation due to event and pre-event waters having essentially the same concentration (analysis not shown). This is consistent with previous work demonstrating that stable water isotopes have proven less useful in snowmelt-dominated, seasonally arid environments where recharge is dominated by snowmelt (Earman et al., 2006), and thus indistinguishable from event water (Jin, Siegel, Lautz, & Lu, 2012). Regardless, other process-relevant information may be gained by exploiting the isotopic signatures and variability in the translation of snowmelt to streamflow during different discharge conditions to elucidate controls on runoff generation.

# 6. CONCLUSIONS

Specific Conductance (SC) recorded in our study watersheds showed large amounts of dilution in peak streamflow periods indicating that seasonal snowmelt dominated annual streamflow contributions. Streamflow and SC also showed distinct hysteretic patterns at annual and daily scales. Annually, most hysteresis indices that could be identified were negative, suggesting faster flow pathways dominated streamflow on the rising limb of the annual hydrograph compared to slower flow pathways occurring during the falling limb. During snowmelt-induced diurnal cycles, SC-Q hysteresis was consistently negative, indicating the daily melt water with the lowest SC preferentially contributed to streamflow on the falling limb of diurnal streamflow cycles after throughflow water was displaced. Hysteresis indices derived from SC-Q relationships were significantly correlated to proportions of quickflow and surficial geology, supporting the idea that the youngest fraction of runoff controlled stream water solute concentration dynamics in these systems.

#### Data Availability Statement

The data that support the findings of this study are available from the corresponding author upon reasonable request.

# LITERATURE CITED

Atwood W. W. (1937). Records of Pleistocene Glaciers in the Medicine Bow and Park Ranges. *The Journal of Geology*, 45(2), 113–140. DOI: 10.1086/624513

Benettin P., Bailey S. W., Rinaldo A., Likens G. E., McGuire K. J., & Botter G. (2017). Young runoff fractions control streamwater age and solute concentration dynamics. *Hydrological Processes*, 31(16), 2982–2986. DOI: 10.1002/hyp.11243

Brown L. E., Hannah D. M., & Milner A. M. (2007). Vulnerability of alpine stream biodiversity to shrinking glaciers and snowpacks. *Global Change Biology*, 13(5), 958-966. DOI: 10.1111/j.1365-2486.2007.01341

- Broxton P. D., Troch P. A., & Lyon S. W. (2009). On the role of aspect to quantify water transit times in small mountainous catchments. *Water Resources Research*, 45(8), 1–15. DOI: 10.1029/2008WR007438
- Buttle J. M. (1994). Isotope hydrograph separations and rapid delivery of pre-event water from basins drainage. *Physical Geography*, 18(1), 16–41.
- Buttle J. M., Webster K. L., Hazlett P. W., & Jeffries D. S. (2019). Quickflow response to forest harvesting and recovery in a northern hardwood forest landscape. *Hydrological Processes*, 33(1), 47–65. DOI: 10.1002/hyp.13310
- Caine N. (1989). Hydrograph separation in a small alpine basin based on inorganic solute concentrations. *Journal of Hydrology*, 112, 89–101.
- Caine N. (1992). Modulation of the diurnal streamflow response by the seasonal snowcover of an alpine basin.  $Journal\ of\ Hydrology$ , 137(1–4), 245–260. DOI: 10.1016/0022-1694(92)90059-5
- Caissie D., Pollock T. L., & Cunjak R. A. (1996). Variation in stream water chemistry and hydrograph separation in a small drainage basin. *Journal of Hydrology*, 178(1–4), 137–157. DOI: 10.1016/0022-1694(95)02806-4
- Carroll R. W. H., Bearup L. A., Brown W., Dong W., Bill M., & Williams K. H. (2018). Factors controlling seasonal groundwater and solute flux from snow-dominated basins. *Hydrological Processes*, 32(14), 2187–2202. DOI: 10.1002/hyp.13151
- Carroll R. W. H., Deems J. S., Niswonger R., Schumer R., & Williams K. H. (2019). The Importance of Interflow to Groundwater Recharge in a Snowmelt-Dominated Headwater Basin. *Geophysical Research Letters*, 46(11), 5899–5908. DOI: 10.1029/2019GL082447
- Case J. C., Arneson C. S., & Hallberg L. L. (1998). Preliminary 1:500,000-scale digital surficial geology map of Wyoming. Wyoming State Geological Survey.
- Cross W. P. (1949). The relation of geology to dry-weather stream flow in Ohio. Eos, Transactions American Geophysical Union, 30(4), 563–566. DOI: 10.1029/TR030i004p00563
- Dadic R., Mott R., Lehning M., & Burlando P. (2010). Wind influence on snow depth distribution and accumulation over glaciers. *Journal of Geophysical Research: Earth Surface*, 115(1), 1–8. DOI: 10.1029/2009JF001261
- Dunne T., Black R. D. (1971). Runoff Processes during Snowmelt. Water Resources Research, 7 (5), 1160–1172. DOI: 10.1029/WR007i005p01160
- Earman S., Campbell A. R., Phillips F. M., & Newman B. D. (2006). Isotopic exchange between snow and atmospheric water vapor: Estimation of the snowmelt component of groundwater recharge in the southwestern United States. *Journal of Geophysical Research*, 111(9), 1–18. DOI: 10.1029/2005JD006470
- Elder K., Dozier J., & Michaelsen J. (1991). Snow Accumulation and distribution in an alpine watershed. Water Resources Research, 27(7), 1541–1552.
- Evans C, & Davies T. D. (1998). Causes of concentration/discharge hysteresis and its potential as a tool for analysis of episode hydrochemistry. Water Resources Research, 34(1), 129–137. DOI: 10.1029/97WR01881
- Fullhart A. T., Kelleners T. J., Chandler D. G., McNamara J. P., & Seyfried M. S. (2019). Bulk density optimization to determine subsurface hydraulic properties in Rocky Mountain catchments using the GEOtop model. *Hydrological Processes*, 33(17), 2323–2336. DOI: 10.1002/hyp.13471
- Genereux D. (1998). Quantifying uncertainty in tracer-based hydrograph separations. Water Resources Research, 34(4), 915–919. DOI: 10.1029/98WR00010
- Godsey S. E., Kirchner J. W., & Clow D. W. (2009). Concentration—discharge relationships reflect chemostatic characteristics of US catchments. *Hydrological Processes*, 23, 1844–1864. DOI: 10.1002/hyp

- Hall F. R. (1968). Base-Flow Recessions—A Review. Water Resources Research , 4(5), 973–983. DOI: 10.1029/WR004i005p00973
- Hamlet A. F., Mote P. W., Clark M. P., & Lettenmaier D. P. (2005). Effects of temperature and precipitation variability on snowpack trends in the Western United States. *Journal of Climate*, 18(21), 4545–4561. DOI: 10.1175/JCLI3538.1
- Hewlett J. D. (1961). Soil moisture as a source of base flow from steep mountain watersheds. U.S. Forest Service, Southeastern Forest Experiment Station Paper # 132.
- Hewlett J. D., & Hibbert A. R. (1967). Factors affecting the response of small watershed to precipitation in humid areas. Forest Hydrology, 275–279. DOI: 10.1177/0309133309338118
- Homer C., & Fry J. (2016). The National Land Cover Database. US Geological Survey Fact Sheet (February): 1–4 Available at: http://pubs.usgs.gov/fs/2012/3020/.
- Huth A. K., Leydecker A., Sickman J. O., & Bales R. C. (2004). A two-component hydrograph separation for three high-elevation catchments in the Sierra Nevada, California. *Hydrological Processes*, 18(9), 1721–1733. DOI: 10.1002/hyp.1414
- Intergovernmental Panel on Climate Change (IPCC). 2013. Climate Change: The Physical Science Basis, Working Group 1 Contribution to the Fifth Assessment Report of the Intergovernmental Panel on Climate Change. Cambridge, United Kingdom.
- Jantze E. J., Laudon H., Dahlke H. E., & Lyon S. W. (2015). Spatial Variability of Dissolved Organic and Inorganic Carbon in Subarctic Headwater Streams. *Arctic, Antarctic, and Alpine Research*, 47(3), 529–546. DOI: 10.1657/AAAR0014-044
- Jasechko S., Jean Birks S., Gleeson T., Wada Y., Fawcett P., Sharp Z., ... Welker J. (2014). The pronounced seasonality of global groundwater recharge.  $Water\ Resources\ Research$ , 50, 8845–8867. DOI: 10.1002/2014WR015829
- Jin L., Siegel D. I., Lautz L. K., & Lu Z. (2012). Identifying streamflow sources during spring snowmelt using water chemistry and isotopic composition in semi-arid mountain streams.  $Journal\ of\ Hydrology$ , 470–471, 289–301. DOI: 10.1016/j.jhydrol.2012.09.009
- Kobayashi D. (1986). Separation of a snowmelt hydrograph by stream conductance.  $Journal\ of\ Hydrology$ , 84, 157–165.
- Kronholm S. C., & Capel P. D. (2015). A comparison of high-resolution specific conductance-based endmember mixing analysis and a graphical method for baseflow separation of four streams in hydrologically challenging agricultural watersheds. *Hydrological Processes*, 29(11), 2521–2533. DOI: 10.1002/hyp.10378
- Kurylyk B. L., & Hayashi M. (2017). Inferring hydraulic properties of alpine aquifers from the propagation of diurnal snowmelt signals.  $Water\ Resources\ Research$ , 53(5), 4271–4285. DOI: 10.1002/2016WR019651
- Laudon H., Sjöblom V., Buffam I., Seibert J., & Mörth M. (2007). The role of catchment scale and landscape characteristics for runoff generation of boreal streams. Journal~of~Hydrology~,~344(3–4),~198–209.~DOI:~10.1016/j.jhydrol.2007.07.010
- Lewis W. M., & Grant M. C. (1979). Relationships between stream discharge and yield of dissolved substances from a Colorado mountain watershed.  $Soil\ Science\ ,\ 128(6),\ 353-363.$
- Li D., Wrzesien M. L., Durand M., Adam J., & Lettenmaier D. P. (2017). How much runoff originates as snow in the western United States, and how will that change in the future?  $Geophysical\ Research\ Letters$ , 44(12), 6163–6172. DOI: 10.1002/2017GL073551
- Liu F., Williams M. W., & Caine N. (2004). Source waters and flow paths in an alpine catchment, Colorado Front Range, United States. *Water Resources Research*, 40(9), 1–16. DOI: 10.1029/2004WR003076

- Lloyd C. E. M., Freer J. E., Johnes P. J., & Collins A. L. (2016). Using hysteresis analysis of high-resolution water quality monitoring data, including uncertainty, to infer controls on nutrient and sediment transfer in catchments. *Science of the Total Environment*, 543, 388–404. DOI: 10.1016/j.scitotenv.2015.11.028
- Loheide S. P., & Lundquist J. D. (2009). Snowmelt-induced diel fluxes through the hyporheic zone. Water Resources Research, 45(7), 1–9. DOI: 10.1029/2008WR007329
- Lundquist J. D., & Cayan D. R. (2002). Seasonal and Spatial Patterns in Diurnal Cycles in Streamflow in the Western United States. Journal of Hydrometeorology, 3(5), 591–603. DOI: 10.1175/1525-7541(2002)003<0591:SASPID>2.0.CO;2
- Lundquist J. D., & Dettinger M. D. (2005). How snowpack heterogeneity affects diurnal streamflow timing. Water Resources Research, 41(5), 1–14. DOI: 10.1029/2004WR003649
- Lundquist J. D., & Flint A. L. (2006). Onset of Snowmelt and Streamflow in 2004 in the Western United States: How Shading May Affect Spring Streamflow Timing in a Warmer World. *Journal of Hydrometeorology*, 7 (6), 1199–1217. DOI: 10.1175/jhm539.1
- Lytle D. A., & Poff N. L. (2004). Adaptation to natural flow regimes. *Trends in Ecology & Evolution*, 19(2), 94–100.
- McCabe G. J., Wolock D. M., Pederson G. T., Woodhouse C. A., & McAfee S. (2017). Evidence that Recent Warming is Reducing Upper Colorado River Flows. *Earth Interactions*, 21(10). DOI: 10.1175/EI-D-17-0007.1
- McNamara J., Kane D. L., & Hinzman L. D. (1997). Hydrograph separation in an Arctic watershed using mixing model and graphical techniques. *Water Resources Research*, 33(7), 1707–1719.
- McNamara J. P., Chandler D., Seyfried M., & Achet S. (2005). Soil moisture states, lateral flow, and streamflow generation in a semi-arid, snowmelt-driven catchment. *Hydrological Processes*, 19(20), 4023–4038. DOI: 10.1002/hyp.5869
- Miller M. P., Buto S. G., Susong D. D., & Rumsey C. A. (2016). The importance of base flow in sustaining surface water flow in the Upper Colorado River Basin. Water Resources Research , 52(5), 3547-3562. DOI: 10.1002/2015WR017963
- Miller M. P., Susong D. D., Shope C. L., Heilweil V. M., & Stolp B. J. (2014). Continuous estimation of base-flow in snowmelt-dominated streams and rivers in the Upper Colorado River Basin: A chemical hydrograph separation approach.  $Water\ Resources\ Research$ , 50(8), 6986–6999. DOI: 10.1002/2013WR014939
- Molotch N. P., Brooks P. D., Burns S. P., Litvak M., Monson R. K., Mcconnell J. R., & Musselman K. (2009). Ecohydrological controls on snowmelt partitioning in mixed-conifer sub-alpine forests. *Ecohydrology*, 2, 129–142. DOI: 10.1002/eco.48
- Mueller M. H., Weingartner R., & Alewell C. (2013). Importance of vegetation, topography and flow paths for water transit times of base flow in alpine headwater catchments. Hydrology and Earth System Sciences, 17(4), 1661-1679. DOI: 10.5194/hess-17-1661-2013
- Mugo J. M., & Sharma T. C. (1999). Application of a conceptual method for separating runoff components in daily hydrographs in Kimakia forest catchments, Kenya. *Hydrological Processes*, 13(17), 2931–2939, DOI: 10.1002/(SICI)1099-1085(19991215)13:17<2931::AID-HYP838>3.0.CO;2-N
- Munn L. C., & Arneson C. S. (1998). Soils of Albany County, Wyoming. (October): 1–13.
- Musselman K. N., Clark M. P., Liu C., Ikeda K., & Rasmussen R. (2017). Slower snowmelt in a warmer world. *Nature Climate Change*, 7 (3), 214–219. DOI: 10.1038/nclimate3225
- Mutzner R., Weijs S. V., Tarolli P., Calaf M., Oldroyd H. J., & Parlange M. B. (2015). Controls on the diurnal streamflow cycles in two subbasins of an alpine headwater catchment. Water Resources Research , 51(5), 3403-3418. DOI: 10.1002/2014WR016581

- Nippgen F., McGlynn B. L., Marshall L. A., & Emanuel R. E. (2011). Landscape structure and climate influences on hydrologic response. *Water Resources Research*, 47(12), 1–17. DOI: 10.1029/2011WR011161
- Pellerin B. A., Saraceno J. F., Shanley J. B., Sebestyen S. D., Aiken G. R., Wollheim W. M., & Bergamaschi B. A. (2012). Taking the pulse of snowmelt: In situ sensors reveal seasonal, event and diurnal patterns of nitrate and dissolved organic matter variability in an upland forest stream. *Biogeochemistry*, 108(1–3), 183–198. DOI: 10.1007/s10533-011-9589-8
- Penna D., Tromp-Van Meerveld H. J., Gobbi A., Borga M., & Dalla Fontana G. (2011). The influence of soil moisture on threshold runoff generation processes in an alpine headwater catchment. *Hydrology and Earth System Sciences*, 15(3), 689–702. DOI: 10.5194/hess-15-689-2011
- Pilgrim D. H., Huff D. D., & Steele T. D. (1979). Use of specific conductance and contact time relations for separating flow components in storm runoff. Water Resources Research , 15(2), 329-339. DOI: 10.1029/WR015i002p00329
- Pinder G. F., & Jones J. F. (1969). Determination of the ground-water component of peak discharge from the chemistry of total runoff. Water Resources Research, 5(2), 438–445. DOI: 10.1029/WR005i002p00438
- PRISM Climate Group OSU. 2019. PRISM Climate Data Available at: http://prism.oregonstate.edu.
- Qin Y., Abatzoglou J. T., Siebert S., Huning L. S., AghaKouchak A., Mankin J. S., . . . Mueller N. D. (2020). Agricultural risks from changing snowmelt. *Nature Climate Change*, 10, 459-465. DOI: 10.1038/s41558-020-0746-8
- Reitz M., Sanford W. E., Senay G. B., & Cazenas J. (2017). Annual Estimates of Recharge, Quick-Flow Runoff, and Evapotranspiration for the Contiguous U.S. Using Empirical Regression Equations. *Journal of the American Water Resources Association*, 53(4), 961–983. DOI: 10.1111/1752-1688.12546
- Roberge J., & Plamondon A. P. (1987). Snowmelt runoff pathways in a boreal forest hillslope, the role of pipe throughflow. *Journal of Hydrology*, 95(1–2), 39–54. DOI: 10.1016/0022-1694(87)90114-4
- Rood S. B., Pan J., Gill K. M., Franks C. G., Samuelson G. M., & Shepherd A. (2008). Declining summer flows of Rocky Mountain rivers: Changing seasonal hydrology and probable impacts on floodplain forests. *Journal of Hydrology*, 349(3–4), 397–410. DOI: 10.1016/j.jhydrol.2007.11.012
- Rumsey C. A., Miller M. P., Susong D. D., Tillman F. D., & Anning D. W. (2015). Regional scale estimates of baseflow and factors influencing baseflow in the Upper Colorado River Basin. *Journal of Hydrology: Regional Studies*, 4, 91–107. DOI: 10.1016/j.ejrh.2015.04.008
- Segura C., Noone D., Warren D., Jones J. A., Tenny J., & Ganio L. M. (2019). Climate, Landforms, and Geology Affect Baseflow Sources in a Mountain Catchment. *Water Resources Research*, 55(7), 5238–5254. DOI: 10.1029/2018WR023551
- Singh V. P. (1997). Effect of spatial and temporal variability in rainfall and watershed characteristics on stream flow hydrograph.  $Hydrological\ Processes$ , 11(12), 1649–1669. DOI: 10.1002/(SICI)1099-1085(19971015)11:12<1649::AID-HYP495>3.0.CO;2-1
- Sklash M. G., & Farvolden R. N. (1979). The role of groundwater in storm runoff. Journal of Hydrology ,  $43,\ 45-65$ . DOI: 10.1016/S0167-5648(09)70009-7
- Spence C. (2007). On the relation between dynamic storage and runoff: A discussion on thresholds, efficiency, and function. Water Resources Research , 43(12), 1–11. DOI: 10.1029/2006WR005645
- Stewart I. T., Cayan D. R., & Dettinger M. D. (2005). Changes toward earlier streamflow timing across western North America. *Journal of Climate*, 18(8), 1136–1155. DOI: 10.1175/JCLI3321.1
- Tague C., Grant G., Farrell M., Choate J., & Jefferson A. (2008). Deep groundwater mediates streamflow response to climate warming in the Oregon Cascades. *Climatic Change*, 86(1–2), 189–210. DOI:

10.1007/s10584-007-9294-8

Thayer D., Parsekian A. D., Hyde K., Speckman H., Beverly D., Ewers B., ... Holbrook, W.S. (2018). Geophysical Measurements to Determine the Hydrologic Partitioning of Snowmelt on a Snow-Dominated Subalpine Hillslope. *Water Resources Research*, 54(6), 3788–3808. DOI: 10.1029/2017WR021324

Tromp-Van Meerveld H. J., McDonnell J. J. (2006). Threshold relations in subsurface stormflow: 2. The fill and spill hypothesis. *Water Resources Research*, 42(2), 1–11. DOI: 10.1029/2004WR003800

Uchida T., Tromp-Van Meerveld I., McDonnell J. J. (2005). The role of lateral pipe flow in hillslope runoff response: An intercomparison of non-linear hillslope response. *Journal of Hydrology*, 311(1–4), 117–133. DOI: 10.1016/j.jhydrol.2005.01.012

Varhola A., Coops N. C., Weiler M., Moore R. D. (2010). Forest canopy effects on snow accumulation and ablation: An integrative review of empirical results. *Journal of Hydrology*, 392(3–4), 219–233. DOI: 10.1016/j.jhydrol.2010.08.009

Vivoni E. R., Rinehart A. J., Mendez-Barroso L. A., Aragon C. A., Bisht G., Cardenas M. B, ... Wyckoff, R. L. (2008). Vegetation controls on soil moisture distribution in the Valles Caldera, New Mexico, during the North American monsoon. *Ecohydrology*, 1, 225–238. DOI: 10.1002/eco.11

Webb R. W., Fassnacht S. R., Gooseff M. N. (2018). Hydrologic flow path development varies by aspect during spring snowmelt in complex subalpine terrain. *Cryosphere*, 12(1), 287–300. DOI: 10.5194/tc-12-287-2018

Williams M. W., Seibold C., Chowanski K. (2009). Storage and release of solutes from a subalpine seasonal snowpack: Soil and stream water response, Niwot Ridge, Colorado. Biogeochemistry, 95(1), 77–94. DOI: 10.1007/s10533-009-9288-x

Woelber B., Maneta M. P., Harper J., Jencso K. G., Gardner W. P, Wilcox C., Lopez-moreno I. (2018). The influence of diurnal snowmelt and transpiration on hillslope throughflow and stream response. *Hydrology and Earth System Sciences*, 22, 4295-4310. https://doi.org/10.5194/hess-22-4295-2018

Wyoming State Geological Survey. (2014). Wyoming Bedrock Geology. Laramie, WY.

Table 1: Study watershed topographic characteristics. South-facing refers to percent of watershed area with aspect facing south (aspect = 157.5 - 202.5 degrees). North-facing refers to percent of watershed area with aspect facing north (aspect = 0 - 22.5, 337.5 - 360 degrees).

Site.ID	Area (km <sup>2</sup> )	Mean elevation (m)	Mean Slope (%)	South-facing (%)	North-facing (%)	Stream length (
GOLD100	12.5	2950	16.5	12.5	19.7	27.7
LIBB100	21.2	3201	18.3	19.0	12.5	39.2
LIBB200	21.9	3192	18.7	19.1	13.0	41.9
LIBB400	48.2	3058	19.3	17.5	15.6	98.8
NASH100	5.03	3239	18.2	23.9	5.9	13.2
NASH200	22.6	3123	18.9	24.5	7.6	53.7
NFLL100	37.3	3032	17.2	17.7	4.3	64.7
NFLL200	63.0	3050	18.7	19.9	5.4	127.3
NONM100	0.53	2993	26.2	26.1	7.3	2.3

Table 2: Surficial geology (percent of total watershed area) of study watersheds.

Site.ID	Glaciated bedrock	Glaciated deposits	Grus / alluvium	Landslide / slopewash	Residuum / alluvium S
GOLD100	0.0	8.3	52.6	0.0	25.9

Site.ID	Glaciated bedrock	Glaciated deposits	Grus / alluvium	Landslide / slopewash	Residuum / alluvium S
LIBB100	39.7	60.3	0.0	0.0	0.0
LIBB200	37.6	62.4	0.0	0.0	0.0
LIBB400	18.5	56.9	13.3	0.0	6.3
NASH100	35.5	64.5	0.0	0.0	0.0
NASH200	46.9	53.1	0.0	0.0	0.0
NFLL100	8.6	76.6	1.2	3.1	7.0
NFLL200	21.3	68.2	0.7	1.9	4.3
NONM100	1.6	98.4	0.0	0.0	0.0

Table 3: Baseflow separation results (%) with associated uncertainty from Eq. 3.

	Rising limb	Rising limb	Peak flow	Peak flow	Falling limb	Falling limb	Low flow	Lo
Site.ID	Direct Runoff	Baseflow	Direct Runoff	Baseflow	Direct Runoff	Baseflow	Direct Runoff	В
GOLD100	$85.8 \pm 18.8$	$14.2 \pm 18.8$	$89.2 \pm 19.5$	$10.8 \pm 19.5$	$87.0 \pm 19.1$	$13.0 \pm 19.1$	$6.6 \pm 5.1$	93
LIBB100	$67.5 \pm 14.0$	$32.5 \pm 14.0$	$71.7 \pm 14.7$	$28.3 \pm 14.7$	$70.0 \pm 14.4$	$30.0 \pm 14.4$	$10.2 \pm 6.6$	89
LIBB200	$70.5 \pm 15.9$	$29.5 \pm 15.9$	$71.9 \pm 16.2$	$28.1 \pm 16.2$	$68.6 \pm 15.5$	$31.4 \pm 15.5$	$7.3 \pm 5.5$	92
LIBB400	$77.0 \pm 17.5$	$23.0 \pm 17.5$	$77.2 \pm 17.6$	$22.8 \pm 17.6$	$70.1 \pm 16.1$	$29.9 \pm 16.1$	$8.4 \pm 5.7$	91
NASH100	$70.9 \pm 8.7$	$29.1 \pm 8.7$	$71.0 \pm 8.7$	$29.0 \pm 8.7$	$67.2 \pm 8.3$	$32.8 \pm 8.3$	$34.4 \pm 6.0$	65
NASH200	$66.4 \pm 7.6$	$33.6 \pm 7.6$	$72.5 \pm 8.2$	$27.5 \pm 8.2$	$67.9 \pm 7.7$	$32.1 \pm 7.7$	$24.3 \pm 4.0$	75
NFLL100	$72.3 \pm 9.6$	$27.7 \pm 9.6$	$80.8 \pm 10.6$	$19.2 \pm 10.6$	$76.6 \pm 10.1$	$23.4 \pm 10.1$	$14.6 \pm 3.9$	85
NFLL200	$66.1 \pm 8.9$	$33.9 \pm 8.9$	$73.2 \pm 9.8$	$26.8 \pm 9.8$	$69.7 \pm 9.3$	$30.3 \pm 9.3$	$15.2 \pm 3.8$	84
NONM100	$68.5 \pm 18.8$	$31.5 \pm 18.8$	$76.1 \pm 20.7$	$23.9 \pm 20.7$	$71.1 \pm 19.4$	$28.9 \pm 19.4$	$11.5\pm7.1$	88

Table 4: Mean baseflow, quickflow, and through flow, and total runoff amounts in mm (and % of total runoff) from 2016-2018.

Site.ID	Baseflow	Quickflow	Throughflow	Total	Peak flow	Low flow
GOLD100	57 (22%)	33 (13%)	168 (65%)	258	122 (47%)	4.8 (1.8%)
LIBB100	250(36%)	98 (14%)	348 (50%)	696	323 (46%)	9.6 (1.4%)
LIBB200	192 (37%)	74 (14%)	259 (46%)	524	246 (47%)	7.4 (1.4%)
LIBB400	176 (33%)	69 (13%)	289 (54%)	533	252 (47%)	8.8 (1.6%)
NASH100	274 (38%)	52 (7%)	401 (55%)	727	288 (40%)	19(2.6%)
NASH200	208 (42%)	43 (9%)	250 (50%)	501	186 (37%)	13~(2.6%)
NFLL100	94 (36%)	28 (11%)	139 (53%)	261	102 (39%)	7.8 (3.0%)
NFLL200	162 (40%)	46 (11%)	199 (49%)	407	182 (41%)	8.1 (2.0%)
NONM100	139~(46%)	24 (8%)	142~(47%)	305	128 (42%)	$8.2\ (2.7\%)$

Table 5: Quickflow and throughflow as a percentage of direct runoff during the snowmelt period and annually. The mean diurnal (%) during the snowmelt period was also calculated.

	Snowmelt	Snowmelt	Annual	Annual	
Site.ID	Quickflow	Throughflow	Quickflow	Throughflow	Mean diurnal
GOLD100	20.4	79.6	16.4	83.6	31.4
LIBB100	27.7	72.3	21.9	78.1	33.5
LIBB200	25.7	74.3	22.1	77.9	31.3
LIBB400	23.0	77.0	19.3	80.7	30.3
NASH100	15.4	84.6	11.4	88.6	19.7
NASH200	19.8	80.2	14.5	85.5	24.0
NFLL100	20.7	79.3	17.0	83.0	27.9
NFLL200	22.2	77.8	18.7	81.3	27.7
NONM100	17.8	82.2	14.7	85.3	23.1

Table 6: Annual and daily hysteresis indices for study watersheds. Annual hysteresis indices were calculated at the 10<sup>th</sup> (HI10), 25<sup>th</sup> (HI25), and 50<sup>th</sup> (HI50) discharge percentiles. Daily hysteresis indices were calculated for each day during the snowmelt period at the 25<sup>th</sup>, 50<sup>th</sup>, and 75<sup>th</sup> discharge percentiles. We averaged each date's hysteresis indices and grouped them by hydrograph period below.

	Annual hysteresis index	Annual hysteresis index	Annual hysteresis index	Daily hysteresis index	Daily hysteresis index	Daily hysteresis index	Daily hysteresis index
Site.ID	HI10	HI25	HI50	HI Rising	HI Peak flow	HI Falling	HI Snowmelt
GOLD100	0.061	0.055	0.044	0.150	0.086	-0.016	0.073
LIBB100	-0.166	-0.174	-0.132	0.102	0.118	0.130	0.117
LIBB200	-0.190	-0.144	-0.057	-0.042	0.238	0.357	0.184
LIBB400	-0.197	-0.167	-0.116	0.119	0.162	0.241	0.174
NASH100	0.018	0.054	0.110	0.109	0.015	-0.036	0.029
NASH200	0.214	0.082	0.053	0.268	0.180	0.038	0.162
NFLL100	0.022	-0.016	0.010	0.291	0.284	0.267	0.281
NFLL200	0.122	0.030	0.011	0.350	0.263	0.192	0.268
NONM100	-0.444	-0.172	0.033	0.113	0.095	-0.081	0.047

Table 7: Correlation matrix (Pearson's r) between watershed properties, runoff mechanisms. Shades of red and blue indicate negative and positive correlations, respectively. Darker shades indicate significant correlations. Bold values with \*,\*\*,\*\*\* indicate significant correlations with p-values less than 0.10, 0.05, and 0.01, respectively.

	Watershed property	Watershed property	Watershed property	Watershed property	Watershed
Variable	Glacial deposits (%)	Mean elevation	Mean snow depth	Mean precip.	North-facin
South-facing (%)	0.37	0.34	0.33	0.28	-0.68**
Glacial deposits		0.09	0.11	-0.01	-0.76**
Mean Elevation			0.99 ***	0.99 ***	-0.19
Mean snow depth				0.98 ***	-0.13

	Watershed property	Watershed property	Watershed property	Watershed property	Watershed
Mean precipitation					-0.08
North-facing $(\%)$					
Baseflow (%)					
Quickflow (%)					
Throughflow (%)					
Mean total runoff					
Mean runoff ratio					
Annual HI25					

Figure 1: Digital elevation model, location of study watersheds and snow measurement sites. Elevation was calculated at 0.5 m resolution from a LIDAR flight in October, 2014.

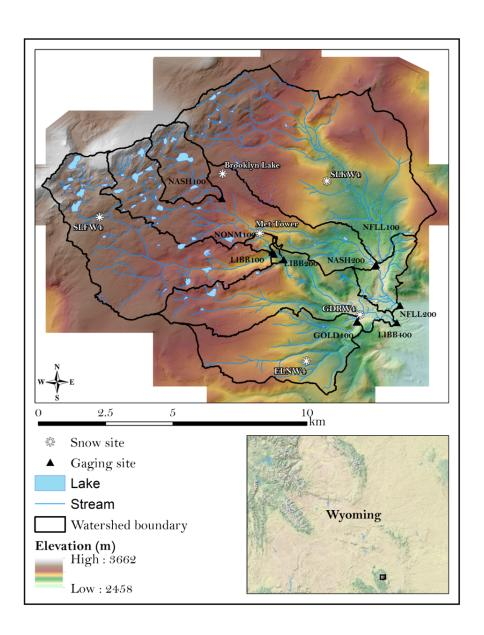
Figure 2: Baseflow separation example for GOLD100 (a) and NONM100 (b). Baseflow (red) is separated from total streamflow (black) using Eq. 2. Direct runoff (blue) is calculated by subtracting baseflow from total streamflow.

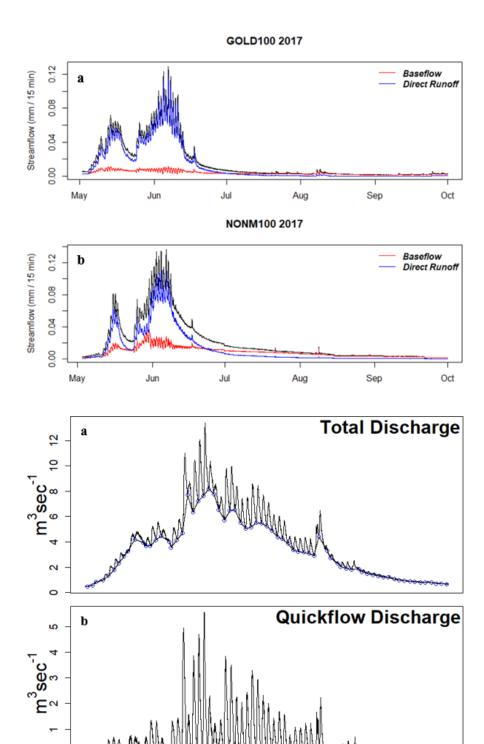
Figure 3: Quickflow hydrograph separation example for LIBB400 during the 2018 snowmelt period. Quickflow discharge (b) is subtracted from total streamflow discharge (a) based on natural occurring snowmelt-induced diurnal cycles. Inflection points (a; blue circles) used to extract quickflow were identified with a computer code when instantaneous streamflow curvature was at a daily maximum.

Figure 4: Three-component hydrograph separation for LIBB400 during 2018. Green represents baseflow separated from the total hydrograph using a mass-balance method. Blue and red represent two components of direct runoff: throughflow and quickflow, respectively.

Figure 5: Normalized discharge (black) and specific conductance (blue) for GOLD100 (a) and NONM100 (b) in 2017. Specific conductance vs. streamflow for GOLD100 (c) and NONM100 (d) in 2017. Color denotes the day of the water year.

Figure 6: Time series of streamflow (blue) and specific conductance (red) for NFLL200 during peak flow conditions (a). Dashed lines show the timing of daily peak streamflow and how they relate to the timing of specific conductance. The solid lines show how specific conductance is typically lower on the falling limb of diurnal streamflow cycles compared to the same recorded streamflow value on the rising limb. Daily normalized SC – Q plots during the rising limb (b) and falling limb (c) along with the daily hysteresis index (HI25). Colors denote hour past noon for respective dates with arrows denoting the direction of hysteresis.





Jun

Jul

